

1 **Predictive modelling of rainfall-induced**
2 **landslide hazard in the Lesser Himalaya of**
3 **Nepal**

4 Ranjan Kumar Dahal. Shuichi Hasegawa. Atsuko Nonomura. Minoru Yamanaka .
5 Santosh Dhakal . Pradeep Poudyal

6 R. K. Dahal

7 *1 Dept. of Safety Systems Construction Engineering, Faculty of Engineering, Kagawa*
8 *University, 2217-20, Hayashi-cho, Takamatsu City, 761-0396, Japan*

9 *2 Department of Geology, Tri-Chandra Multiple Campus, Tribhuvan University,*
10 *Ghantaghar, Kathmandu, Nepal*

11 Phone: 0081-87-864-2140

12 Fax: 0081-87-864-2031

13 Email: ranjan@ranjan.net.np

14 URL: <http://www.ranjan.net.np>

15 S. Hasegawa . A. Nonomura . M. Yamanaka .

16 *Dept. of Safety Systems Construction Engineering, Faculty of Engineering, Kagawa*
17 *University, 2217-20, Hayashi-cho, Takamatsu City, 761-0396, Japan*

18

19 Santosh Dhakal

20 *Department of Mines and Geology, Lainchaur, Kathmandu, Nepal*

21

22 Pradeep Poudyal

23 *Mountain Risk Engineering Unit, Tribhuvan University, Kirtipur, Kathmandu Nepal*

24

25 **Abstract**

26 Landslide hazard mapping is a fundamental tool for disaster management activities in mountainous
27 terrains. The main purpose of this study was to evaluate the predictive power of weights-of-evidence
28 modelling in landslide hazard assessment in the Lesser Himalaya of Nepal. Weights-of-evidence
29 modelling was applied as predictive modelling, within a geographical information system (GIS), to
30 derive a landslide hazard map of the south-western marginal hills of Kathmandu Valley, Lesser
31 Himalaya, Nepal. Thematic maps representing various factors (e.g., slope, aspect, relief, flow
32 accumulation, distance to drainage, soil depth, engineering soil type, landuse, geology, distance to road
33 and mean annual rainfall) that are related to landslide activity were generated, using field data and GIS
34 techniques, at a scale of 1:10,000. Landslide events of the 1970s, 1980s, and 1990s were used to assess
35 the Bayesian probability of landslides in each cell unit with respect to the causative factors. To assess
36 the accuracy of the resulting landslide hazard map, this map was correlated with a map of landslides
37 triggered by the 2002 extreme rainfall events. The accuracy of the map was evaluated by various
38 techniques, including area under the curve, success rate and prediction rate. The resulting landslide

39 hazard value calculated from the old landslide data showed greater than 80% prediction accuracy. The
40 analysis suggests that geomorphology-based and human intervention-related causative factors have
41 significant roles in the variance of the probability value in comparison to geology-related factors.
42 Finally, after rectification of the landslide hazard value of new landslides from old landslides, a
43 landslide hazard map with greater than 88% prediction accuracy was prepared. The methodology
44 appears to have extensive applicability in the Lesser Himalaya of Nepal, with the limitation that the
45 model's performance is contingent on the availability of data from past landslides.

46 **1 Introduction**

47 Landslides are among the most damaging natural hazards in the mountainous terrains
48 of the Lesser Himalaya of Nepal. Sites that are particularly at risk for landslides
49 should therefore be identified so as to reduce damage in the region. Landslide hazard
50 assessment has become a vital subject for authorities responsible for infrastructural
51 development and environmental protection. Much research has been carried out to
52 prepare landslide susceptibility and landslide hazard maps. According to Varnes
53 (1984), landslide hazard can be assessed in terms of probability of occurrence of a
54 potentially damaging landslide phenomenon within a specified period of time and
55 within a given area. Both intrinsic and extrinsic variables affect landslide hazards in
56 an area (Siddle et al., 1991; Wu and Siddle, 1995; Atkinson and Massari, 1998; Dai et
57 al., 2001; Çevik and Topal, 2003). The intrinsic variables determining landslides
58 hazards include bedrock geology, geomorphology, soil depth, soil type, slope
59 gradient, slope aspect, slope curvature, elevation, engineering properties of the slope
60 material, land use pattern, drainage patterns, and so on. Similarly, extrinsic variables
61 include heavy rainfall, earthquakes, and volcanoes. Observations and experience show
62 that the probability of landslide occurrence depends on both intrinsic and extrinsic
63 variables. However, extrinsic variables are site specific and possess a temporal
64 distribution. In landslide hazard assessment practice, the term “landslide susceptibility
65 mapping” is used when the extrinsic variables are not considered while determining
66 the probability of occurrence of a landslide event (Dai et al., 2001). In this research, a
67 landslide hazard map was prepared by considering the extrinsic variable of rainfall in
68 addition to the intrinsic variables.

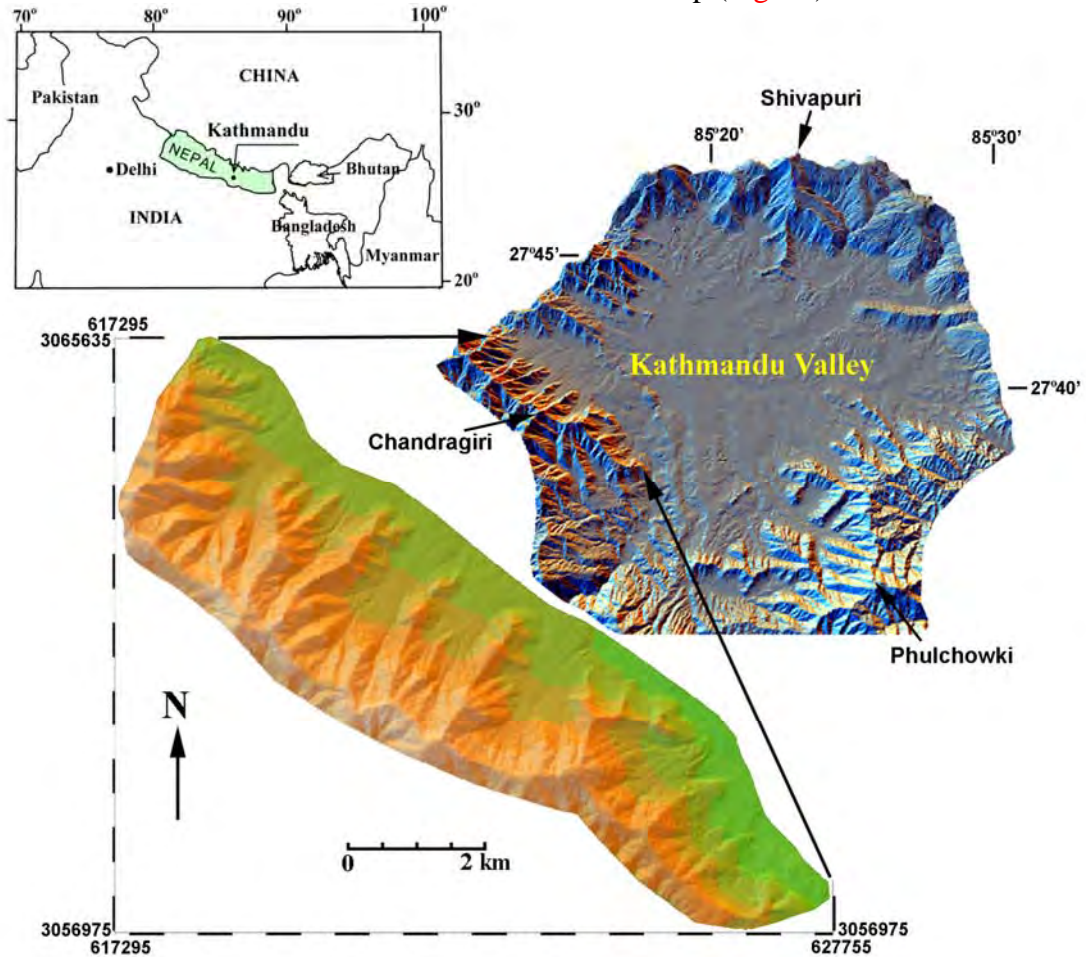
69 There have been numerous studies involving landslide hazard evaluation, and most
70 deal mainly with landslide susceptibility. In particular, Guzzetti et al. (1999) evaluated
71 many cases of landslide hazard studies. Landslide hazard may also be assessed
72 through heuristic, deterministic, and statistical approaches (Yin and Yan 1988; Van
73 Westen and Terlien 1996; Gökçeoglu and Aksoy, 1996; Pachauri et al., 1998; Van
74 Westen 2000; Lee and Min 2001; Dai et al., 2001; Van Westen et al., 2003; Zêzere et
75 al., 2004; Süzen and Doyuran, 2004; Saha et al., 2005, Dahal et al., 2007; Sharma and
76 Kumar, 2007). A heuristic approach is a direct or semi direct mapping methodology in
77 which a direct relationship is established between the occurrence of slope failures and
78 the causative factors during the landslide inventory. Therefore, in this approach the
79 opinions of experts are very important in estimating landslide potential from the data
80 involving intrinsic variables. Similarly, assigning weight values and ratings to the
81 variables is very subjective and the results are often not reproducible. Deterministic

82 approaches, however, are based on slope stability analyses, and are only applicable
83 when the ground conditions are relatively homogeneous across the study area and the
84 landslide types are known. The infinite slope stability model has been widely used to
85 assess landslide hazard in deterministic approaches (Wu and Sidle 1995; Terlien 1996;
86 Gökceoglu and Aksoy 1996), and such stability models need a high degree of
87 simplification of the intrinsic variables. Statistical approaches, on the other hand, are
88 indirect hazard mapping methodologies that involve statistical determination of the
89 combinations of variables that have led to landslide occurrence in the past. All
90 possible intrinsic variables are entered into a Geographical Information System (GIS)
91 and integrated with a landslide inventory map. Both bivariate and multivariate
92 statistical methods have been used widely in such approaches to landslide hazard
93 mapping (Siddle et al.1991; Atkinson and Massari 1998; Van Westen 2000; Dai et al.,
94 2001; Dahal et al., 2007; Neuhäuser and Terhorst, 2007). Keeping this in mind, in this
95 study the landslide hazard was evaluated through GIS techniques using weights-of-
96 evidence modelling with respect to a bivariate statistical approach. The study area in
97 the south-western hills of Kathmandu Valley suffered extensive landslide damage
98 during the heavy monsoon rainfall of 2002, and thus is a suitable ideal site for the
99 evaluation of rainfall-induced landslide hazard in the Lesser Himalaya of Nepal.
100 Various models have been applied to landslide susceptibility and hazard mapping in
101 the last 25 years (Guzzetti et al., 1999; Chung and Fabbri, 2003; Remondo et al 2003;
102 Van Westen et al., 2003; Lee 2004). In the most of the landslide susceptibility and
103 hazard mappings, independent validation of statistical models for landslide hazard or
104 susceptibility assessment is lacking. A time-based separation of landslides can be
105 most appropriate for validation; in fact, use of older landslides for modelling and new
106 landslides for validation is the most acceptable method of validation (Van Westen et
107 al., 2003). One of the objectives of the present study is to overcome this deficiency,
108 and in the existing research the same landslide data were used for both hazard
109 assessment and validation. The main objectives of this paper are: 1) to employ
110 weights-of-evidence modelling with a bivariate statistical approach to define the
111 physical parameters contributing to the occurrence of landslides in the Lesser
112 Himalaya and 2) to prepare a classified landslide hazard map that possesses high
113 prediction and success rates for the study area.

114 **2 The study area**

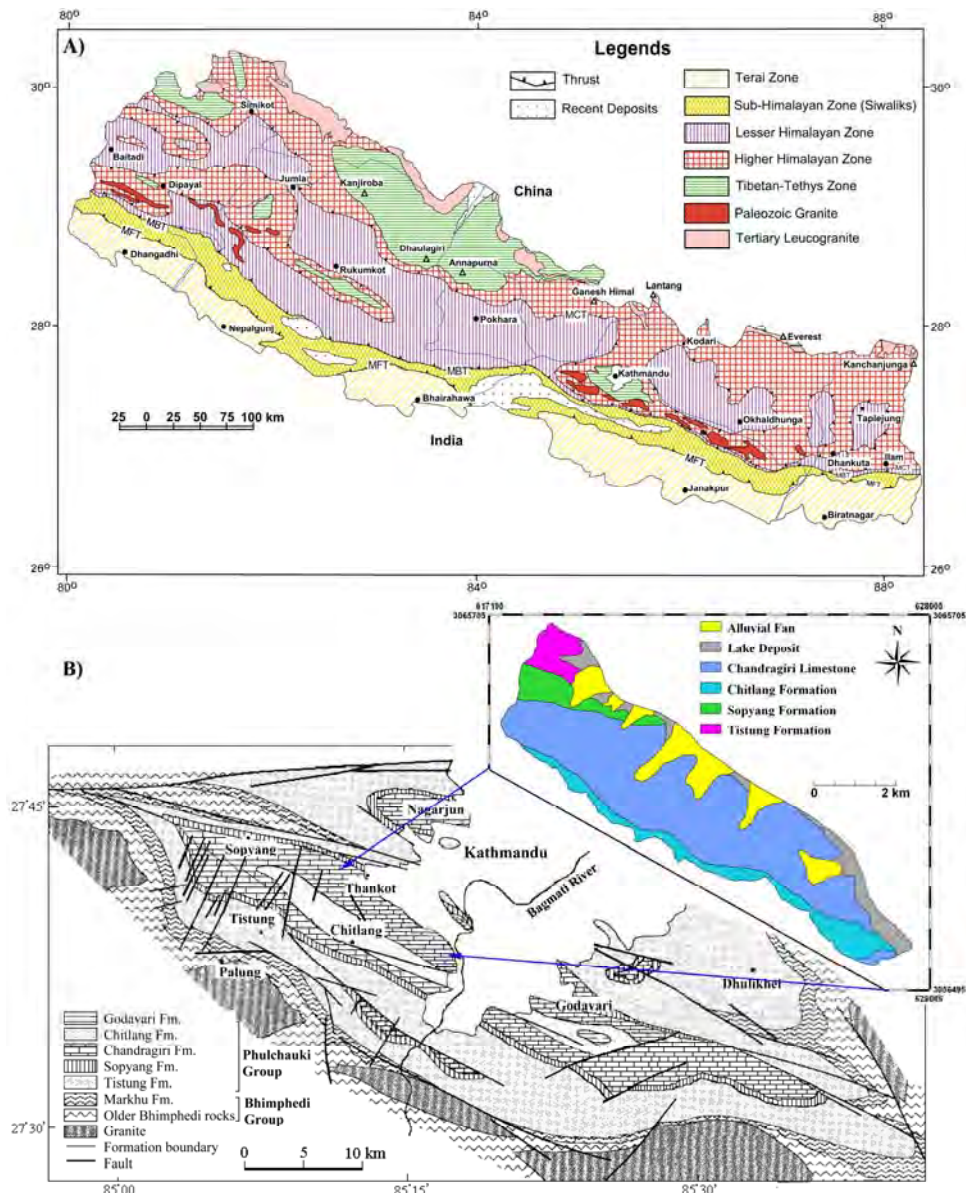
115 The study area is located in the south-western hills of the Kathmandu Valley, Lesser
116 Himalaya, Nepal (Fig. 1). The Kathmandu Valley is the largest intermountain basin of
117 the Lesser Himalayan Zone of the Himalaya (Ganser, 1964), and is surrounded by
118 high rising mountain ranges such as Shivapuri (2732 m) in the north, Phulchowki
119 (2762 m) in the southeast, and Chandragiri (2543 m) in the southwest. Geologically,
120 Nepal is divided into five tectonic zones from north to south: the Tibetan-Tethys
121 Himalayan Zone, Higher Himalayan Zone, Lesser Himalayan Zone, Siwalik Zone,
122 and Terai Zone (Fig 2A). Among these five zones, the Lesser Himalayan Zone and
123 Siwalik Zone are the most prone to landslides in the monsoon period. The study area
124 is within the Lesser Himalaya and belongs to the Phulchauki and Bhimphedi groups,

125 which together form the Kathmandu Complex (Stöcklin 1980). The Bhimphedi Group
126 consists of relatively high-grade metamorphic rocks of Precambrian age, whereas the
127 Phulchauki Group is composed of weakly metamorphosed sediments of early to
128 middle Palaeozoic age. The southern hills of the Kathmandu Valley consist of
129 intensely folded and faulted metasediments, mainly limestone with a subordinate
130 amount of shale and sandstone of the Phulchauki Group (Fig 2B).



131
132 Fig 1. Location map of the study area
133
134

135
136
137
138
139
140



141

142 Fig. 2. A) Geological map of Nepal (modified after Amatya and Jnawali, 1994, and
 143 Dahal 2006a) and B) Geological map of south of Kathmandu valley (modified after
 144 Stöcklin and Bhattarai, 1977) and geological map of study area is shown in inset.

145

146 The study area ranges in elevation from 1400 m to 2,560 m, with an area of 18.9 km².
 147 The mean annual precipitation of area ranges from 1500 to 2200 mm. Most of the
 148 slope faces north, and the slope gradient generally increases with increasing elevation.
 149 Colluvium is the main slope material above the bedrock. The area consists mainly of a
 150 dense forest of immature trees and thorny shrubs. In 2002, the study area experienced
 151 extreme events of monsoon rainfall and faced huge losses of life and property. On
 152 July 23, 2002, monsoon rains dropped 300.1 mm of rain in a 24-h period. This was the
 153 highest precipitation in the area in the last 36 years. These rainfall events triggered 73
 154 debris slides in the study area. Debris flows also occurred after the sliding. A single
 155 landslide occurred near the central part of the study area, killing 16 people (Dahal et
 156 al., 2006b). According to the disaster history of the area and interviews with local

157 residents, the 2002 disaster was the one of the worst natural disasters of that area in
158 the last 50 years.

159 The area is on the outskirts of Kathmandu Metropolitan city in Nepal, and settlement
160 at the base of the hills has risen sharply over the last 10 years. Because of the
161 panoramic view of the Himalayas to the north, many housing projects have been
162 constructed without any consideration of landslide hazards. Some research has been
163 conducted regarding landslide risk in the study area. Paudel (2003) described a
164 disaster management scenario for the central part of the study area, giving examples
165 of the disastrous landslides of 2002. Paudyal and Dhital (2005) performed a statistical
166 risk analysis for the southern part of Kathmandu, including the study area, and
167 categorized the levels of risk as low, moderate and high. Dahal et al. (2006b) provided
168 a comprehensive description of the study area with respect to rainfall and landslides.

169 **3 Weights-of-evidence modelling**

170 In this study, weights-of-evidence modelling was used for the landslide hazard
171 mapping. The weights-of-evidence modelling technique uses the Bayesian probability
172 model, and was originally developed for mineral potential assessment (Bonham-
173 Carter et al., 1988, 1989; Agterberg 1992; Agterberg et al., 1993; Bonham-Carter,
174 2002). Several authors have applied the weights-of-evidence method to mineral
175 potential mapping using GIS (Emmanuel et al., 2000; Harris et al., 2000; Tangestani
176 and Moore 2001). Cheng (2004) used this method to predict the location of flowing
177 wells, whereas Daneshfar and Benn (2002) used the method to analyse spatial
178 associations between faults and seismicity. Zahiri et al. (2006) used weights-of-
179 evidence modelling for mapping of cliff instabilities associated with mine subsidence.
180 This method has also been applied to landslide susceptibility mapping (Lee et al.,
181 2002; Van Westen et al., 2003, Lee and Choi 2004, Lee and Sambath 2006; Dahal et
182 al., 2007; Sharma and Kumar, 2007; Neuhäuser and Terhorst, 2007).

183 A detailed description of the mathematical formulation of the method is available in
184 Bonham-Carter (2002). The method calculates the weight for each landslide causative
185 factor based on the presence or absence of the landslides within the area. The related
186 mathematical relationships are described below.

187 Favourability of an incidence of landslide given the presence of the causative factor
188 can be expressed by conditional probability (Bonham-Carter, 2002) as follows:

189
$$P\{L|F\} = \frac{P\{L \cap F\}}{P\{F\}} \dots\dots\dots (1)$$

190 where $P(L|F)$ is the conditional probability of the presence of a landslide (L) given
191 the presence of a causative factor, F . But $P\{L \cap F\}$ is equal to the proportion of the
192 total area occupied by L and F together, so:

193
$$P\{L \cap F\} = \frac{N\{L \cap F\}}{N\{A\}} \dots\dots\dots (2)$$

194 and prior probability of landslide occurrence can be expressed by

195 $P\{F\} = \frac{N\{F\}}{N\{A\}}$ (3)

196 where $P\{F\}$ and $N\{F\}$ are the probability and area of causative factor, respectively.
 197 Similarly, $N\{A\}$ is the total area of the region (Fig 3). Substituting Eq. (2) and Eq. (3)
 198 into Eq. (1) gives:

199 $P\{L|F\} = \frac{N\{L \cap F\}}{N\{F\}}$ (4)

200 In order to obtain an expression relating the posterior probability of L in terms of the
 201 prior probability and a multiplication factor, the conditional probability of being on F ,
 202 given the presence of landslide, is defined as follows:

203 $P\{F|L\} = \frac{P\{F|L\}}{P\{L\}}$ (5)

204 But $P\{F \cap L\}$ is the same as $P\{L \cap F\}$, Eq. (1) and Eq. (5) can be combined to get
 205 $P\{L|F\}$, satisfying the relationship as follows:

206 $P\{L|F\} = P\{L\} \frac{P\{F|L\}}{P\{F\}}$ (6)

207 Eq. (6) reveals that the conditional or posterior probability of the landslide, given the
 208 presence of the causative factor, is equal to the prior probability of the landslide $P\{L\}$
 209 multiplied by the factor $P\{F \cap L\} / P\{F\}$. A similar expression can be derived for the
 210 posterior probability of landslide occurring given the absence of the causative factor
 211 as follows:

212 $P\{L|\bar{F}\} = P\{L\} \frac{P\{\bar{F}|L\}}{P\{\bar{F}\}}$ (7)

213 where \bar{L} is the absence of landslide and \bar{F} is the absence of the landslide causative
 214 factor.

215 The probability model described here can be also expressed in odds form (Bonham-
 216 Carter, 2002). Weights-of-evidence modelling uses the natural logarithm of odds
 217 known as log odds or *Logits*. To convert Eq. (6) to odds, both sides are divided
 218 by $P\{\bar{L}|F\}$, leading to:

219 $\frac{P\{L|F\}}{P\{\bar{L}|F\}} = \frac{P\{L\}}{P\{\bar{L}\}} \frac{P\{F|L\}}{P\{F\}}$ (8)

220 But from the definitions of conditional probability:

221 $P\{\bar{L}|F\} = \frac{P\{\bar{L} \cap F\}}{P\{F\}} = \frac{P\{F|\bar{L}\} P\{\bar{L}\}}{P\{F\}}$ (9)

222 Rearranging Eq. (8) and (9) gives the following equation:

223 $\frac{P\{L|F\}}{P\{\bar{L}|F\}} = \frac{P\{L\}}{P\{\bar{L}\}} \frac{P\{F\}}{P\{F\}} \frac{P\{F|L\}}{P\{F|\bar{L}\}}$ (10)

224 Likewise, the odds of the presence of a landslide can be expressed as follows:

225 $O\{L\} = \frac{P\{L\}}{1 - P\{L\}}$ (11)

226 and

227 $O\{L\} = \frac{P\{L\}}{P\{\bar{L}\}}$ (12)

228 Substituting the odds into Eq. (10) and cancelling leads to:

229 $O\{L|F\} = O\{L\} \frac{P\{F|L\}}{P\{F|\bar{L}\}}$ (13)

230 where $O\{L|F\}$ is the conditional or posterior odds of a landslide given a causative
 231 factor. $O\{L\}$ is the prior odds of a landslide and $P\{F|L\}/P\{F|\bar{L}\}$ is known as the
 232 sufficient ratio (*SR*). In weights-of-evidence modelling, when the natural logarithms
 233 of both sides of Eq. (13) are taken, $\log_e SR$ gives positive weights of evidence,
 234 W_i^+ (Bonham-Carter, 2002) and can be expressed as follows:

235 $W_i^+ = \log_e \frac{P\{F|L\}}{P\{F|\bar{L}\}}$ (14)

236 Similarly, for the case of odds, the following relation can be derived:

237 $W_i^+ = \log_e \frac{O\{L|F\}}{O\{L\}}$ (15)

238 Similar algebraic manipulation leads to the derivation of an odds expression for the
 239 conditional probability of landslides given the absence of the causative factor as
 240 follows:

241 $O\{L|\bar{F}\} = O\{L\} \frac{P\{\bar{F}|L\}}{P\{\bar{F}|\bar{L}\}}$ (16)

242 The term $P\{\bar{F}|L\}/P\{\bar{F}|\bar{L}\}$ is called the necessary ratio (*NR*). *SR* and *NR* are also
 243 known as likelihood ratios. In weights of evidence modelling, when the natural
 244 logarithms of both sides of Eq. (16) are taken, the $\log_e NR$ gives negative weights of
 245 evidence, W_i^- , as follows:

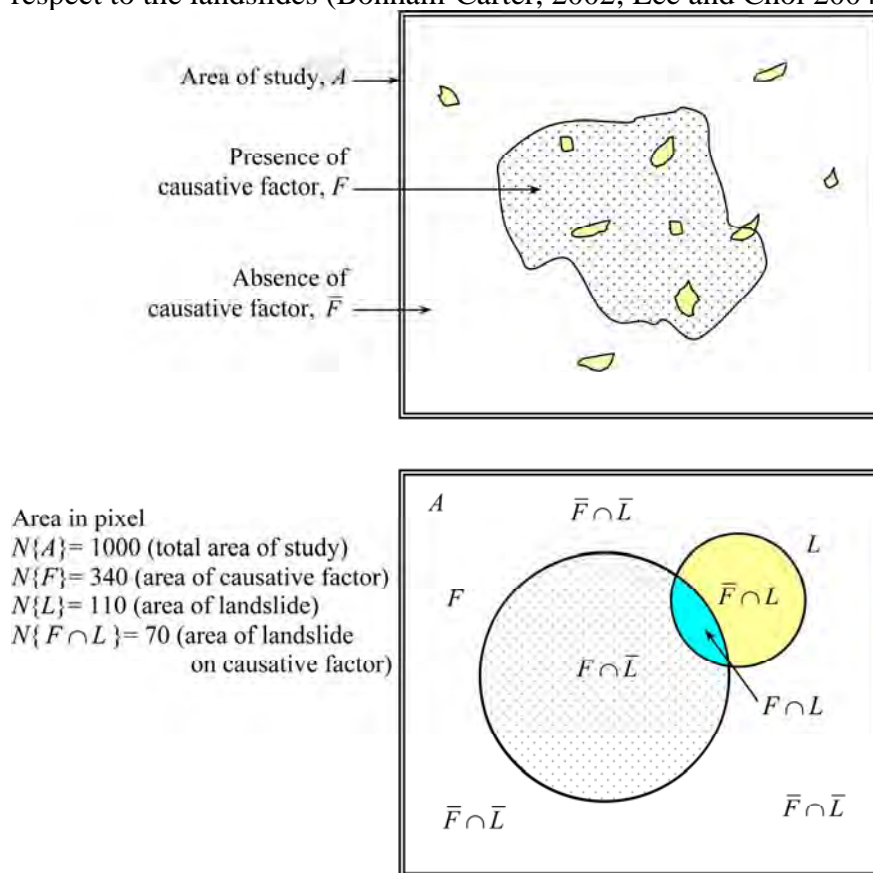
246 $W_i^- = \log_e \frac{P\{\bar{F}|L\}}{P\{\bar{F}|\bar{L}\}}$ (17)

247 Similarly, for the case of odds, the expression is as follows:

248 $W_i^- = \log_e \frac{O\{L|\bar{F}\}}{O\{L\}}$ (18)

249 In this research, the logarithm of likelihood ratios, i.e., Eq. (14) and Eq. (17), were
 250 used to calculate weights from the conditional probability value. A positive weight
 251 (W_i^+) indicates that the causative factor is present at the landslide location, and the
 252 magnitude of this weight is an indication of the positive correlation between presence
 253 of the causative factor and landslides. A negative weight (W_i^-) indicates an absence of
 254 the causative factor and shows the level of negative correlation. The difference
 255 between the two weights is known as the weight contrast, W_f ($W_f = W_i^+ - W_i^-$), and the

256 magnitude of contrast reflects the overall spatial association between the causative
 257 factor and landslides. In weights-of-evidence modelling, the combination of causative
 258 factors assumes that the factors are conditionally independent of one another with
 259 respect to the landslides (Bonham-Carter, 2002; Lee and Choi 2004).



260
 261 Fig. 3. Illustration of weights-of-evidence calculations. Upper figure is an illustration
 262 of a causative factor map that shows the location of landslides, and lower figure is a
 263 Venn diagram summarizing the spatial overlap relationships between the causative
 264 factor and the landslides. Each landslide occupies a small unit area. The total area of
 265 study is shown as a rectangle (in the real field condition, it can be an irregularly
 266 shaped area). The areas of circles are not to scale.

267
 268 In this research, using bivariate statistics, the assumption is made that all landslides in
 269 a given study area occur under the same combination of parameters, and that all sets
 270 of parameters are conditionally independent.

271 Although weights-of-evidence modelling has not been previously applied in landslide
 272 hazard mapping of the Lesser Himalaya of Nepal, the suitability of the technique for
 273 this purpose is evident in its successful use in other studies for examining
 274 susceptibility, spatial relationships, and the distribution of particular features. The area
 275 selected for modelling has typical spatial and physical characteristics. The area
 276 consists of landslides triggered by rainfall, the intrinsic variables are quantifiable in
 277 field, and the production of accurate landslide conditioning factor maps is feasible.

278 Debris slide and debris flow (Varnes 1984) types of landslide have occurred
279 predominantly in the study area. For modelling purposes, only debris slide scars were
280 considered, because weights-of-evidence modelling can only be applied for single
281 types of landslides. All the debris flows in the area were initiated after failure at the
282 upper reaches of topographic hollows. Thus, debris slides were the prime landslide
283 consequence for the study area after rainfall events, and this predictive modelling
284 deals with landslide hazard associated with the areas prone to landslide initiation.
285 For the successful application of weights-of-evidence modelling, historical landslide
286 data are essential; these data are used to estimate the weighting factors that contribute
287 to landslides. This modelling procedure relies on the fundamental assumption that
288 future landslides will occur under conditions and factors equal or similar to those
289 contributing to past landslides. It also assumes that causative factors for the mapped
290 landslides remain constant over time. However, this can be true only for same type of
291 landslide. When different types of landslide are considered, the weights-of-evidence
292 method needs to be applied separately to each landslide type (Neuhäuser and Terhorst,
293 2007).

294 **4 Data preparation**

295 The main steps for landslide hazard mapping were data collection and the construction
296 of a spatial database from which relevant factors were extracted. This was followed
297 by assessment of the landslide hazard using the relationship between landslide and
298 landslide causative factors, and the subsequent validation of results. A key feature of
299 this method is that the possibility of landslide occurrence will be comparable with
300 observed landslides.

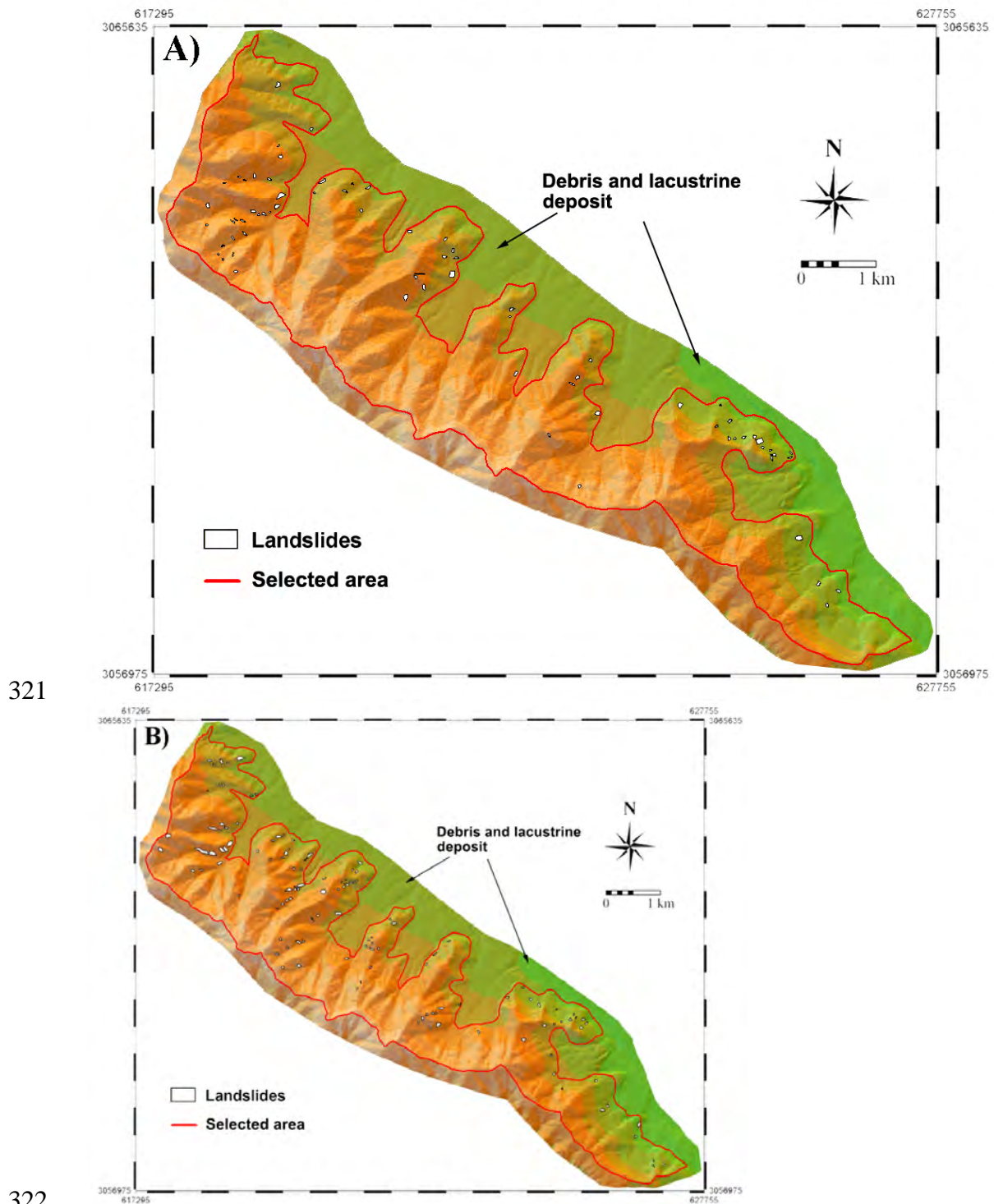
301 For the hazard modelling, a number of thematic data of causative factors were
302 identified, including slope, slope aspect, geology, flow accumulation, relief, landuse,
303 soil type, soil depth, distance to road, and mean annual rainfall. Topographic maps
304 and aerial photographs taken by Department of Survey, Government of Nepal were
305 considered as basic data sources for generating these layers. Field surveys were
306 carried out for data collection and to prepare data layers of various factors, as well as
307 to prepare geological, soil depth, soil type and landuse maps. A landslide distribution
308 map after the 2002 extreme monsoon rainfall events was also prepared in field. These
309 data sources were used to generate various data layers using the GIS software ILWIS
310 3.3. Brief descriptions of each data layer preparation procedure are provided here.

311 **1. Landslide characteristics and inventory maps**

312 A landslide inventory map is the simplest output of direct landslide mapping. It shows
313 the location of discernible landslides. It is a key factor used in landslide susceptibility
314 mapping by weights-of-evidence modelling because the overlay analysis requires an
315 inventory map.

316 Two landslide inventory maps for new and older landslides were prepared. For the
317 new landslide inventory map, landslides occurring after the 2002 rainfall events were
318 recorded in field immediately after the events, and the landslide inventory map was

319 prepared. As a consequence of 2002 extreme rainfall events, a total of 73 debris slide
320 scars were detected in the study area.



323 Fig. 4. Landslide inventory maps of the study area, A) Inventory map prepared after
324 2002 extreme rainfall event, B) Inventory map prepared from aerial photographs of
325 1979, 1989, and 1995.

326
327 For the older landslide maps, aerial photographs from 1979, 1989 and 1995 at scales
328 of 1:25000 and 1:15000 were taken as a data source. Landslide scars were identified
329 with stereoscopes, and the GIS data layer was prepared. Similarly, for 1:15000 scale

330 aerial photographs, epipolar stereo pairs were generated in ILWIS 3.3 and landslide
331 inventory maps were prepared from screen digitisations. Only landslide scars (main
332 failure portions) were used to delineate the landslides. When preparing landslide
333 inventory maps from air photographs, especially the 1979 photos, only landslide scars
334 having no vegetation were delineated from the photographs. Similarly, for the 1989
335 and 1995 photos, the scars were cross checked with older photographs. The delineated
336 landslide scars from aerial photographs were also verified in the field. However, not
337 all the old scars could be observed in the field because of vegetation, but nearly 70%
338 of the scars (especially landslide scars delineated from 1989 and 1995 maps) were
339 easily verified in field. New landslides were also observed within a few old landslide
340 scars. A total of 119 landslide scars were delineated from the 1979, 1989, and 1995
341 photos. Rainfall data from the nearest rainfall station suggested that there were
342 comparatively high monsoon rainfall events in 1978, 1979, 1987, 1988, and 1993.
343 These events might be responsible for triggering these old landslides. The landslide
344 inventory maps of the both new and older landslides are given in Fig. 4. Finally, to
345 check the predictive power of the model in all possible aspects, three (new landslide,
346 old landslides and all landslides) raster maps of the landslide inventory were prepared
347 and analyses were performed.

348 **2. Geological maps**

349 Geology plays an important role in landslide susceptibility and hazard studies because
350 different geological units have different susceptibilities to active geomorphological
351 processes (Anbalagan 1992; Pachauri et al., 1998; Dai et al., 2001). As mentioned in
352 an earlier section, limestone, shale and metasandstone are the main rock types of the
353 study area. For the geological map preparation, previous studies (Stöcklin and
354 Bhattarai 1978, Acharya 2001) were consulted and geological boundaries of
355 formations were checked and modified as per the field observations.

356 **3. Geomorphology related causative factors**

357 A Digital Elevation Model (DEM) representing the terrain is used to generate various
358 geomorphological parameters which influence the landslide activity in an area. Hence,
359 a DEM was prepared with digital contour data procured from the Department of
360 Survey, Government of Nepal. The DEM of the study area was prepared at 10 m × 10
361 m pixel size. From this DEM, geomorphological thematic data layers such as slope,
362 aspect and relative relief, distance to drainage, and flow accumulation were prepared.
363 Slope data layer, an important parameter in slope stability considerations, comprised
364 eight classes. This classification was decided after measuring slope angles of failed
365 slope during landslide inventory mapping of the more new landslides. Field
366 measurements signified that most of the landslides occurred at slope angles between
367 25° and 55°. A total of seven classes, >5°, 5°-15°, 15°-25°, 25°-35°, 35°-45°, 45°-55°,
368 >55°, were used to prepare the slope map. Aspect refers to the direction of maximum
369 slope of the terrain surface. For the study area, it was divided into nine classes,
370 namely, N, NE, E, SE, S, SW, W, NW and Flat. Both slope and aspect maps were
371 prepared in ILWIS 3.3 from the DEM. For calculation of slope and aspect map, height

372 differences in X- and Y-directions were calculated from the DEM and available
373 commands in ILWIS 3.3 were used.

374 Relative relief is another DEM-based derivative, and is defined as the maximum
375 height dispersion of a terrain normalized by its length or area (Oguchi, 1997). In this
376 paper, relative relief is computed as the difference between the maximum and
377 minimum altitudes within the given class of elevation. The relative relief data layer
378 was prepared from the difference in maximum (2500 m) and minimum elevation
379 (1400 m) and was sliced into twelve classes at 100 m elevation difference.

380 In the study area, appearance of landslides was frequent along streams. Thus, distance
381 of the landslide from a stream was considered as another geomorphology-related
382 causative factor. Subsequently, a distance to drainage map was generated as per the
383 hypothesis that landslides may be more frequent along streams, due to groundwater
384 movement towards stream and toe undercutting. In order to produce the map showing
385 distance to drainage, the drainage segment map was rasterised and the distance to the
386 drainage was calculated in meters. The resultant map was then sliced to give a raster
387 map showing distance to drainage divided into six classes. The six classes were 0 – 10
388 m, 10 – 20 m, 20 – 30 m, 30 – 50 m, 50 – 100 m, and >100 m.

389 Following rainfall events, water flows from areas of convex curvature and
390 accumulates in areas of concave curvature. This process is known as flow
391 accumulation and is a measure of the land area that contributes surface water to an
392 area where water can accumulate. This parameter was considered as relevant to this
393 study because it defines the locations of water concentration after rainfall, and those
394 locations are likely to have a high landslide incidence. Flow accumulation can be
395 explained as the number of pixels, or area, which contributes to runoff of a particular
396 pixel. In fact, flow accumulation is a DEM based derivative and a DEM hydro-
397 processing operation in ILWIS 3.3 that calculates flow accumulation of a watershed.
398 For the study area, the flow accumulation map was prepared from the DEM and was
399 divided into eight classes using histogram information and calculated cumulative
400 percentages.

401 **4. Landuse**

402 Landuse is also one of the key factors responsible for the occurrence of landslides,
403 since barren slopes are more prone to landslides. Vegetation prevents erosion due to
404 the natural anchorage provided by the tree roots; thus, vegetated area is less prone to
405 landslides (Greenway 1987; Styczen and Morgan 1995). Based on field observations
406 and mapping, six landuse classes that may have an impact on landslide activity were
407 considered. These classes were dense forest, dry cultivated land, grassland, shrubs,
408 sparse forest, and sparse shrub. The landuse map was prepared in the field on a
409 topographical map at 1:25,000 scale. Subsequently, the landuse data layer was
410 generated as vector polygons and converted to a raster landuse map in GIS.

411 **5. Distance to road**

412 One of the controlling factors for the stability of slopes is road construction activity.
413 In the study area, many landslides occurred along roads and foot trails due to
414 inappropriately cut slopes and drainage from the roads and trails. Thus, a distance to

415 road factor map was generated by rasterizing the road and trail segment map and
416 calculating the distance to the transport routes in meters. The resulting map was then
417 sliced to develop a raster map showing distance to roads divided into seven classes: 0
418 – 10 m, 10 – 20 m, 20 – 30 m, 30 – 50 m, 50 – 100 m, 100 – 200 m, and >200 m.

419 **6. Soil depth and soil type**

420 Soil mapping was performed mainly for estimating soil depth and identifying
421 engineering soil types. For this purpose, the study area was divided into 16
422 topographical mosaics and a topographic mosaic map was prepared. The topographic
423 mosaic map shows a more or less homogeneous topographic unit on the basis of the
424 orientation of contour lines. For the estimation of soil depth within each topographic
425 mosaic, a total of 19 profile lines were fixed with respect to increments of elevation.
426 Along the profile lines, nearby scars of road cut, trail cuts, gully erosion, old
427 landslides, and soil mines were identified and soil depth was measured with a tape
428 measure. Some locations were inaccessible because of thick forest and the absence of
429 trails; in these cases, visual estimates were made from the nearest ridge and valley. In
430 addition, measurements and observations of soil depth were made at random points
431 during field visits. More than 400 observations and estimates (in both cross sections
432 and random points) were made, and point maps of soil depth were prepared on a
433 1:25,000 scale topographic map. This point map was also digitized in ILWIS 3.3. A
434 kriging point interpolation operation was performed to interpolate randomly
435 distributed point values of soil depth and convert them into regularly distributed point
436 values. Before point interpolation, spatial correlation of point data was performed and
437 autocorrelation, spatial variance and semi-variogram values were acquired. The semi-
438 variogram values were used to obtain necessary input parameters (nugget, sill and
439 range) for kriging by generating a rational quadratic semi-variogram model. The soil
440 depth estimated from kriging was validated in the field mainly for locations of rock
441 exposure, and depths were corrected. Lastly, a soil-depth raster map was generated
442 using the slicing method. The study of landslides after the 2002 extreme rainfall
443 events suggested mainly soil depths of 0.5 m to 2 m had maximum susceptibility to
444 failure. There were some failures in zones having 2 to 4 m soil depth as well. Thus,
445 five soil depth classes were established to create thematic layer of soil depth : <1.0 m,
446 1 m - 1.5 m, 1.5 m - 2.5 m, 2.5 m - 4.0 m, and >4 m.

447 The map of engineering soil types was prepared from field observation. Four main
448 types of soil domains were identified: silty gravel, low plastic clay, silty sand and
449 clayey to silty gravel. In accordance with the unified soil classification system (ASTM
450 D 2487-83), the soil domains were named ML, CL, SM and GM to GC, respectively.
451 Rocky terrains were classified as rock domain. The study area mainly consists of ML
452 over the whole area. SM and CL were also recorded, but these soil types were scarce.
453 GM to GC was found mainly on the base of hills as old fan deposits. Soils were tested
454 in the field for soil domain classification in accordance with the field identification
455 procedure of NAVFAC (1986) and USBR (2001).

456 **7. Rainfall map**

457 Rainfall is an extrinsic variable in hazard analysis, and the spatial distribution of mean
 458 annual rainfall is commonly used in statistical hazard analysis. But, the study area has
 459 many landslides triggered by extreme rainfall. Thus, to make this research more
 460 practical, extreme one day rainfall, for 11 stations around Kathmandu valley was used
 461 to prepare an extreme one day rainfall map. First, a point value map of extreme one
 462 day rainfall was prepared, and the spatial distribution of rainfall was calculated
 463 through the application of the inverse distance squared method in ILWIS 3.3. The
 464 resulting map was sliced to give a raster map divided into four classes having 20 mm
 465 intervals and used in hazard calculation.

466 Thus, a total of 11 factors maps (slope, aspect, relief, flow accumulation, soil depth,
 467 engineering soil type, geology, landuse, distance to drainage, distance to road and
 468 extreme one day rainfall) were selected as thematic data layers for analysis.

469 **5 Analysis and Result**

470 To evaluate the contribution of each factor to landslide hazard, both new and old
 471 landslide distribution data layers were compared separately with various thematic data
 472 layers. For this purpose, Eqs. (14) and (17) were written according to numbers of
 473 pixels as follows:

474
$$W_i^+ = \text{Log}_e \frac{\frac{Npix_1}{Npix_1 + Npix_2}}{\frac{Npix_3 + Npix_4}{Npix_3}} \dots\dots\dots (19)$$

475
$$W_i^- = \text{Log}_e \frac{\frac{Npix_2}{Npix_1 + Npix_2}}{\frac{Npix_3 + Npix_4}{Npix_4}} \dots\dots\dots (20)$$

476 where:

477 $Npix_1$ is the number of pixels representing the presence of both a potential landslide
 478 causative factor and landslides;

479 $Npix_2$ is the number of pixels representing the presence of landslides and absence of a
 480 potential landslide causative factor ;

481 $Npix_3$ is the number of pixels representing the presence of a potential landslide
 482 causative factor and absence of landslides;

483 $Npix_4$ is the number of pixels representing the absence of both a potential landslide
 484 causative factor and landslides.

485 All thematic maps were stored in raster format with a pixel size of 10 m × 10 m and
 486 were combined with three landslide inventory maps (new landslides, old landslides
 487 and all landslides) separately for the calculation of the positive and negative weights.
 488 The calculation procedure was written in the form of a script file in ILWIS 3.3,
 489 consisting of a series of GIS command to support Eqs. (19) and (20). Since all of the
 490 maps are multi-class maps containing several classes, the presence of one factor, such

491 as silty soil, implies the absence of the other factors of the same soil type map.
 492 Therefore, in order to obtain the final weight of each factor, the positive weight of the
 493 factor itself was added to the negative weight of the other factors in the same map
 494 (Van Westen et al., 2003). The final calculated weights for new landslides are given in
 495 **Table 1**.

496 Table 1, Computed weights for classes of various data layers based on new landslide occurrences

Domain	Class	Landslide occurrences	% occu.	No. of pixel in domain	% domain	Ratio % of occu./% of domain	Weight W ⁺	Weight W ⁻
1 Slope	<5 degrees	0	0.000	1116	0.592	0.000	-1.865	0.005
	5 to 15 degrees	23	2.122	7893	4.185	0.507	-0.682	0.021
	15 to 25 degrees	154	14.207	30165	15.993	0.888	-0.119	0.021
	25 to 35 degrees	460	42.435	63148	33.479	1.268	0.239	-0.145
	35 to 45 degree	239	22.048	43453	23.037	0.957	-0.044	0.013
	45 to 55 degrees	125	11.531	28820	15.279	0.755	-0.283	0.044
2 Aspect	>55 degrees	83	7.657	14024	7.435	1.030	0.030	-0.002
	Flat	13	1.199	5795	3.072	0.390	-0.944	0.019
	North	95	8.764	54942	29.129	0.301	-2.315	0.230
	North-East	258	23.801	53565	28.399	0.838	-0.178	0.063
	East	375	34.594	40429	21.434	1.614	0.482	-0.184
	South-East	223	20.572	23204	12.302	1.672	0.518	-0.100
	South	114	10.517	5775	3.062	3.435	1.248	-0.080
	South-West	5	0.461	779	0.413	1.117	0.111	0.000
3 Flow accumulation	West	1	0.092	4130	2.190	0.042	-3.172	0.021
	1 Cell	258	23.801	54223	28.747	0.828	-0.190	0.068
	3 Cells	221	20.387	38765	20.552	0.992	-0.008	0.002
	5 Cells	105	9.686	18033	9.561	1.013	0.013	-0.001
	10 Cells	135	12.454	22432	11.893	1.047	0.046	-0.006
	20 Cells	169	15.590	20053	10.631	1.466	0.386	-0.057
	50 Cells	118	10.886	19110	10.132	1.074	0.072	-0.008
	1000 Cells	76	7.011	14108	7.480	0.937	-0.065	0.005
4 Relief	>1000 Cells	2	0.185	1895	1.005	0.184	-1.699	0.008
	<1400 m	33	3.044	4264	2.261	1.347	0.300	-0.008
	1400 m - 1500 m	133	12.269	10149	5.381	2.280	0.832	-0.076
	1500 m - 1600 m	262	24.170	19314	10.240	2.360	0.867	-0.170
	1600 m - 1700 m	197	18.173	26649	14.128	1.286	0.253	-0.049
	1700 m - 1800 m	283	26.107	29473	15.626	1.671	0.517	-0.133
	1800 m - 1900 m	64	5.904	26391	13.992	0.422	-0.866	0.090
	1900 m - 2000 m	25	2.306	20454	10.844	0.213	-1.553	0.092
	2000 m - 2100 m	60	5.535	17397	9.223	0.600	-0.513	0.040
	2100 m - 2200 m	27	2.491	15212	8.065	0.309	-1.179	0.059
	2200 m - 2300 m	0	0.000	11055	5.861	0.000	-4.158	0.060
	2300 m - 2400 m	0	0.000	6448	3.419	0.000	-3.619	0.034
	>2300 m	0	0.000	1813	0.961	0.000	-2.350	0.009
5 Distance to drainages	0 m - 10 m	64	5.904	20770	11.012	0.536	-0.626	0.056
	10 m - 20 m	59	5.443	13654	7.239	0.752	-0.287	0.019
	20 m - 30 m	81	7.472	15592	8.266	0.904	-0.102	0.009
	30 m - 50 m	166	15.314	30517	16.179	0.947	-0.055	0.010
	50 m - 100 m	335	30.904	55137	29.232	1.057	0.056	-0.024
	>100	379	34.963	52949	28.072	1.245	0.221	-0.101
6 Soil depth	<1.0 m	319	29.428	72259	38.310	0.768	-0.265	0.135
	1 m - 1.5 m	357	32.934	65834	34.903	0.944	-0.058	0.030
	1.5 m - 2.5 m	185	17.066	36788	19.504	0.875	-0.134	0.030
	2.5 m - 4.0 m	198	18.266	11614	6.157	2.966	1.099	-0.139
	>4.0 m	25	2.306	2124	1.126	2.048	0.723	-0.012
7 Engineering soil type	CL	0	0.000	4293	2.276	0.000	-3.212	0.022
	GM and GC	254	23.432	33477	17.748	1.320	0.280	-0.072
	ML	732	67.528	137923	73.123	0.923	-0.080	0.190
	SM	3	0.277	7312	3.877	0.071	-2.645	0.037
	Rock	95	8.764	5614	2.976	2.944	1.091	-0.062
8 Geology	Alluvial Fan	19	1.753	2126	1.127	1.555	0.445	-0.006
	Lake Deposit	3	0.277	3184	1.688	0.164	-1.813	0.014
	Chandragiri Limestone	893	82.380	130998	69.451	1.186	0.172	-0.553
	Chitlang Formation	27	2.491	29398	15.586	0.160	-1.839	0.145
	Sopyang Formation	117	10.793	13552	7.185	1.502	0.410	-0.040
	Tistung Formation	25	2.306	9361	4.963	0.465	-0.769	0.028
	Dense Forest	427	39.391	146613	77.730	0.507	-0.683	1.011
9 Landuse	Dry Cultivated	227	20.941	14952	7.927	2.642	0.981	-0.153
	Grassland	0	0.000	1050	0.557	0.000	-1.804	0.005
	Shrubs	1	0.092	2072	1.099	0.084	-2.482	0.010
	Sparse Forest	237	21.863	19823	10.510	2.080	0.739	-0.136
	Sparse Shurb	192	17.712	4109	2.178	8.131	2.138	-0.174
10 Distance to roads	0 m - 10 m	136	12.546	14198	7.527	1.667	0.515	-0.056
	10 m - 20 m	93	8.579	8839	4.686	1.831	0.610	-0.042
	20 m - 30 m	86	7.934	9472	5.022	1.580	0.461	-0.031
	30 m - 50 m	102	9.410	14966	7.935	1.186	0.172	-0.016
	50 m - 100 m	197	18.173	34141	18.101	1.004	0.004	-0.001
	100 m - 200 m	222	20.480	45380	24.059	0.851	-0.162	0.046
	>200	248	22.878	61623	32.671	0.700	-0.358	0.137
11 Extreme one day rainfall	220 mm - 240 mm	406	37.454	69906	37.062	1.011	0.011	-0.006
	240 mm - 260 mm	44	4.059	36751	19.484	0.208	-1.573	0.176
	260 mm - 280 mm	487	44.926	66956	35.498	1.266	0.237	-0.159
	280 mm - 300 mm	147	13.561	15006	7.956	1.705	0.537	-0.063

497

498 The resulting total weights, as shown in table, directly indicate the importance of each
 499 factor. If the total weight is positive, the factor is favourable for the occurrence of
 500 landslides, and if it is negative, it is not favourable. Some of the factors show little
 501 relation to the occurrence of landslides, as evidenced by weights close to zero. For
 502 example, some classes of flow accumulation, when crossed with all three maps,
 503 reveals values that oscillate around zero without any extreme positive or negative
 504 values. This indicates that flow accumulation is a less important predicting factor.
 505 However, it does not mean that the role of flow accumulation must be exempted
 506 absolutely in the modelling, because class domain has some weights. The frequency
 507 ratio (%landslide / %area) helps to assess the relationship between the factors and
 508 landslide occurrences (Lee and Sambath 2006; Dahal et al., 2007). For example, slope
 509 aspects S, SE and SW show high probabilities of landslide occurrences, whereas
 510 northern slopes are less vulnerable. From the field investigations of orientation of rock
 511 joints, it was noticed that slopes having S, SE and SW aspects were mainly dip slopes
 512 and had seepage problems. This relies on the high probability value of landslide
 513 occurrences in S, SE and SW slopes.
 514 The weights are assigned to the classes of each thematic layer, to produce weighted
 515 thematic maps, which are overlaid and numerically added according to Eq. (5) to
 516 produce a Landslide Hazard Index (LHI) map.

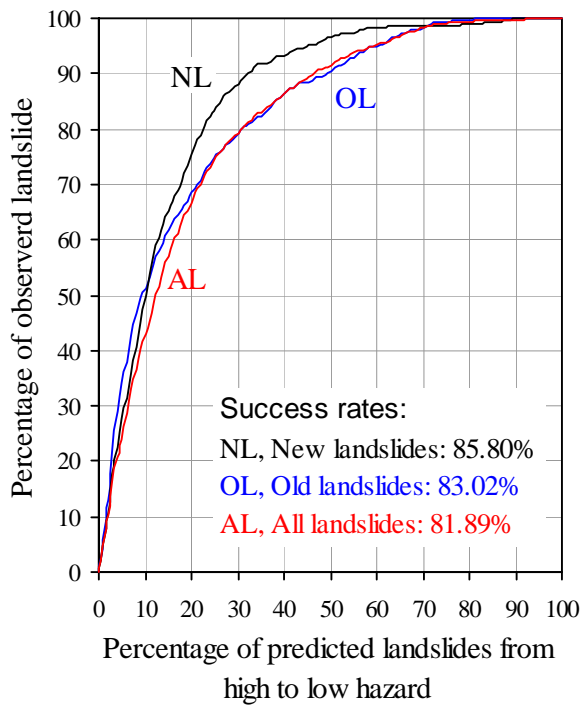
$$517 \quad LHI = W_fSlope + W_fAspcls + W_fFA + W_fRelief + W_fDisdrn + W_fDepth \\
 + W_fEgsoil + W_fgGeo + W_fLanduse + W_fDisrd + W_fRnfall \quad \dots\dots (5)$$

518 where W_fSlope , $W_fAspcls$, W_fFA , $W_fRelief$, $W_fDisdrn$, W_fDepth , $W_fEgsoil$, W_fGeo ,
 519 $W_fLanduse$, W_fDisrd , and $W_fRnfall$ are distribution-derived weights of slope, slope
 520 aspect, flow accumulation, relief, distance to drainages, engineering soil type,
 521 geology, landuse, distance to roads, and extreme one day rainfall factor maps,
 522 respectively. Three attribute maps of different landslide cases were prepared from
 523 respective LHI values. The LHI values were found to lie in the range from -15.662 to
 524 8.231 for the new landslides case, -12.483 to 6.769 for the old landslides case, and -
 525 13.023 to 6.926 for the case of all landslides. The ability of LHI values to predict
 526 landslide occurrences was verified using the success rate curve (Chung and Fabbri,
 527 1999), prediction rate, and effect analysis (Van Westen et al., 2003; Lee, 2004; Dahal
 528 et al., 2007). The success rate indicates what percentage of all landslides occurs in the
 529 classes with the highest value of susceptibility. When old landslides are used for LHI
 530 value calculation and new landslides are used for prediction, the calculated accuracy
 531 rate is called prediction rate (Van Westen et al., 2003; Lee et al., 2007) and is most
 532 suitable parameter for independent validation of the LHI values. Effect analysis helps
 533 to validate and to check the predictive power of selected factors that are used in
 534 hazard analysis.

535 **5.1 Success rates**

536 The success rate curves of all three maps are shown in Fig 5. These curves are
 537 measures of goodness of fit. To obtain the success rate curve for each LHI map, the
 538 calculated index values of all pixels in the maps were sorted in descending order.

539 Then the ordered pixel values were categorised into 100 classes with 1% cumulative
 540 intervals, and classified LHI maps were prepared with the slicing operation in ILWIS
 541 3.3. These classified LHI maps were crossed with the landslide inventory map. Then
 542 the success rate curve was created from the cross table value.



543

544 Fig. 5. Success rate curves of landslide hazard values calculated from three types of
 545 landslide inventory maps. The areas under the curve for all three cases were
 546 determined considering a total area under the curve as $100 \times 100 = 10,000$ units. Other
 547 details are in text.

548

549 In the case of new landslides, the success rate reveals that 10% of the study area
 550 where the LHI had a higher rank could explain 50% of total new landslides. Likewise,
 551 30% of higher LHI value could explain 88% of all landslides. Similarly, for the cases
 552 of old landslides and all landslides, 30% high LHI value could explain about 80% of
 553 total landslides. Fig 5 provides percentage coverage of landslides in various higher
 554 rank percentage of LHI. To compare the landslide hazard results, area under the
 555 curves (Lee, 2004, Dahal et al., 2007) was estimated from the success rate graphs (Fig
 556 5). The area under the curve qualitatively measures the success rate of LHI value. A
 557 total area equal to one denotes perfect prediction accuracy. Similarly, when the area
 558 under the curve is less than 0.5000, the model is invalid. In this study, area under the
 559 curves ranged from 0.8213 to 0.8595. This implies that the success rate ranged from
 560 81% to 86% and the model is valid. Analysis of the new landslide case shows a higher
 561 value of success rate than other two cases.

562 **5.2 Effect analysis**

563 Three landslide hazard maps were prepared by referencing the eleven factor maps. In
564 the weight of evidence modelling, the effect of factor maps is very critical (Lee and
565 Choi, 2004) and effect analysis suggests the predictive power of factor maps.

566 In this weights-of-evidence modelling, however, the combination of causative factors
567 assumes that the factors are conditionally independent of one another with respect to
568 the landslides (Van Westen et al., 2003; Zahiri et al., 2006; Dahal et al.; 2007, Sharma
569 and Kumar, 2007). In previous studies (Lee et al. 2002; Lee and Choi, 2004;
570 Neuhäuser and Terhorst, 2007), conditional independence was described as a
571 precondition for the weights-of-evidence modelling. In this model, we also tested the
572 conditional independency of factors to understand the role of independent factors for
573 acquiring a high success rate. The pair-wise test of conditional independence suggests
574 that out of the 10 intrinsic variables, aspect, flow accumulation, distance to drainage
575 and soil depth reveal conditional independence with Chi-square values less than 2.8.
576 Likewise, the existing research suggests that utilization of geomorphology-related
577 parameters in hazard evaluation is very promising (Van Westen et al., 2003), and
578 geomorphology, geology and human intervention related parameters are considered
579 the most effective hazard evaluation parameters. Thus, a total of five combinations
580 were prepared in order to test the predictive power of geomorphology, geology and
581 human intervention related factors as well as factors showing conditional
582 independence. The following five combinations were selected for the effect analysis.

583 Comb-1: Only geomorphology-related factor maps:

584 This includes W_f Slope, W_f Aspcls, W_f FA, W_f Relief, W_f Disdrn, and W_f Rnfall.

585 Comb-2: Geomorphology and geology-related factors maps:

586 This includes W_f Slope, W_f Aspcls, W_f FA, W_f Relief, W_f Disdrn, W_f Depth,
587 W_f Egsoil, W_f Geo, and W_f Rnfall.

588 Comb-3: Geomorphology and human interventions-related factor maps:

589 This includes W_f Slope, W_f Aspcls, W_f FA, W_f Relief, W_f Disdrn, W_f Landuse,
590 W_f Disrd, and W_f Rnfall

591 Comb-4: Geology and human interventions-related factor maps:

592 This includes W_f Depth, W_f Egsoil, W_f Geo, W_f Landuse, W_f Disrd, and W_f Rnfall

593 Comb-5: Factor maps showing conditional independence:

594 This includes W_f Aspcls, W_f FA, W_f Depth, W_f Disdrn, and W_f Rnfall

595 Being an extrinsic variable, the rainfall factor map was used in all combinations, and
596 landslide hazard values were calculated.

597 To compare the landslide hazard value of all five combinations along with the all
598 factors map (calculated as per Eq. 5); both success rate and prediction rate were
599 calculated from the rate graphs. Four cases of landslide maps were considered and
600 hazard value comparisons were made. These cases include Case I: LHI value of new
601 landslides crossed with same landslide map; Case II: LHI value of old landslides
602 crossed with same landslide map; Case III: LHI value of all landslides crossed with
603 same landslide map; Case IV: LHI value of old landslides crossed with new landslide
604 map. Case I, Case II, and Case III suggest success rates similar to the resulting LHI
605 values. The validation of LHI values from success rate is common in previous studies

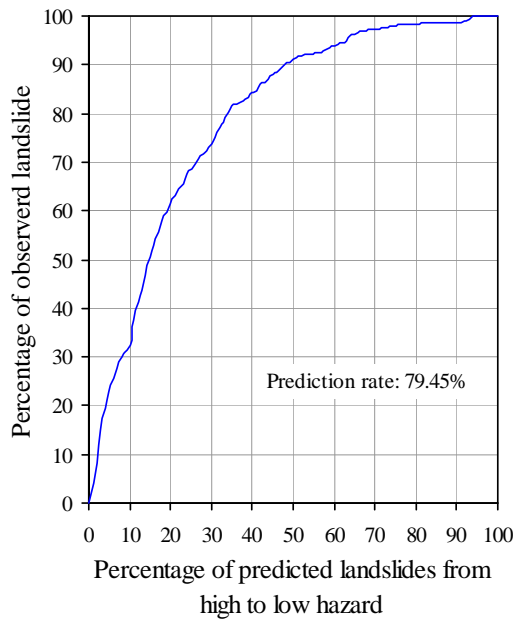
606 of this kind due to a lack of time-based landslide data. In this study, however, both old
 607 and new landslide inventory maps were available and independent validation of LHI
 608 value was possible through the calculation of a prediction rate. Thus, Case IV was the
 609 most informative validation procedure. The success rates of Case I, Case II and Case
 610 III, as well as prediction rates of Case IV, were evaluated by means of area under the
 611 curve, and results are given in **Table 2**.
 612 Table 2, Area under the curve and success rate of all cases and combinations after weights-of-evidence
 613 modelling. Details are in text.

Cases	Scenarios	All maps	Comb-1	Comb-2	Comb-3	Comb-4	Comb-5	
I	LHI value of new landslides crossed with same landslide map	Ratio of the area under the curve	0.858	0.800	0.833	0.840	0.800	0.749
		Sucess rate (%)	85.802	79.994	83.254	83.974	80.015	74.884
II	LHI value of old landslides crossed with same landslide map	Ratio of the area under the curve	0.830	0.788	0.810	0.812	0.694	0.765
		Sucess rate (%)	83.030	78.778	81.024	81.206	0.694	76.542
III	LHI value of all landslides crossed with same landslide map	Ratio of the area under the curve	0.819	0.774	0.798	0.804	0.729	0.746
		Sucess rate (%)	81.889	77.370	79.794	80.382	72.936	74.570
IV	LHI value of old landslides crossed with new landslide map	Ratio of the area under the curve	0.795	0.704	0.744	0.767	0.664	0.677
		Prediction rate (%)	79.454	70.401	74.357	76.745	66.411	67.668

614

615 **Table 2** shows that the success rates of this modelling procedure varied from 66% to
 616 86%. Case I with all factor map combinations shows the maximum success rates.
 617 Similarly, Case I, Case II and Case III have lower success rates in Comb-5 (factor
 618 maps showing conditional independence). This implies that when using weights-of-
 619 evidence modelling for landslide hazard mapping, considering only conditional
 620 independent factors may not be effective for achieving a high success rate for
 621 landslide hazard values. Likewise, geomorphology and human intervention-related
 622 factor maps (Comb-3) show high success rates.

623 The prediction rate in Case IV is also similar to the success rates of Case I, Case II
 624 and Case III with various combinations of maps. Case IV is independent and
 625 established a ratio of area under the curve of 0.7945 when all maps were combined for
 626 the LHI calculation. Thus, there was 79.45% prediction accuracy in LHI value
 627 calculated from old landslides (**Fig 6**). More than 74% of new landslides were well
 628 covered by 30% of high value of LHI calculated from old landslides. **Fig 7**
 629 demonstrates predicted landslide percentages in 10%, 50% and 70% of high value
 630 LHI for various combinations of factor maps. Similarly, Comb-2, Com-3 and the all
 631 maps combinations showed better coverage of predicted landslides in the 30% high
 632 value of landslide hazard.



633

634 Fig. 6. Prediction rate curves of landslide hazard values calculated from old landslide
635 inventory maps

636

637 **5.3 Classified hazard map**

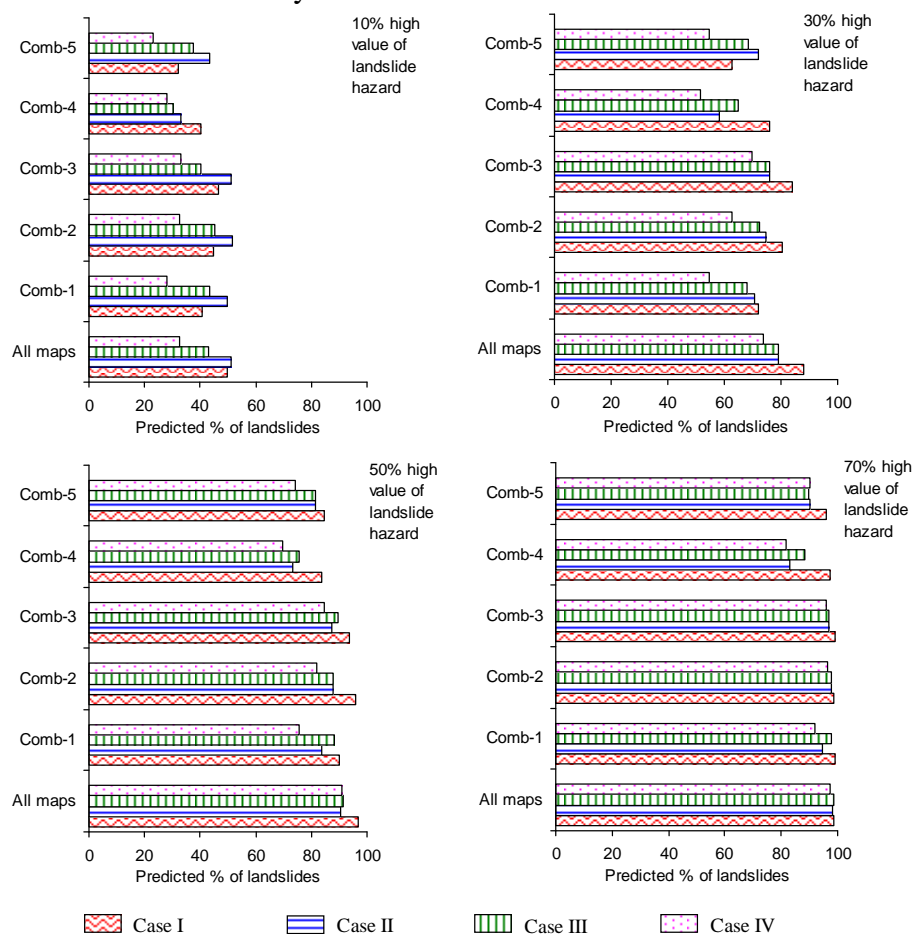
638 For the purpose of classified hazard maps, reference to prediction rate curves (see Fig
639 6) was made and corresponding values of LHI in classes 30%, 50%, 70% and 90%
640 LHI value were selected for hazard classification. Total five landslide hazard classes,
641 very low (less than 30% class of low to high LHI value), low (30% - 50% class of low
642 to high LHI value), moderate (50% - 70% class of low to high LHI value), high (70%
643 - 90% class of low to high LHI value), and very high (more than 90% class of low to
644 high LHI value, i.e., most higher LHI values) were established. On the basis of 30%,
645 50%, 70% and 90% of low to high LHI value, two classified hazard maps were
646 prepared for LHI values of new landslides (Map 1) and for LHI value of old landslides
647 (Map 2).

648 Although Map 1 showed a high success rate, it is not considered the best hazard map
649 for the study area because its prediction rate could not be estimated. Similarly, Map 2
650 also could not be used as final hazard map although its prediction rate was determined
651 because Map 1 consisted of considerable amount of high hazard value cells with
652 respect to same spatial distribution cells of Map-2. Therefore, realizing the
653 distribution of higher value hazard cells in both maps, Map 1 was rectified from high
654 landslide hazard values of Map 2, and a modified landslide hazard map was prepared.
655 For this purpose, cells having very high hazard, high hazard, moderate hazard and low
656 hazard classes of Map 2 were transferred to Map 1 with the help of commands and
657 operations in ILWIS 3.3. In this process, a remarkable number of cells having very
658 low hazard, low hazard and moderate hazard classes in Map 1 were transferred to a
659 high hazard class. The resulting hazard map was again compared with the new

660 landslide case as an estimate of success rate. The resulting success rate curve shows
 661 that the goodness of fit is very high (88.4%) and area under the curve is 0.8840 (Fig.
 662 8). Similarly, in this landslide hazard map, if 20% of the classes have high landslide
 663 hazard value for future landslides, 81% of the landslides can be correctly fit. The final
 664 landslide hazard classification map for the study area, after weights-of-evidence
 665 modelling, is given in Fig 9. Similarly, Table 3 illustrates the distribution of old and
 666 new landslides in the classified hazard map, and the results are very promising. In
 667 total, Very High Hazard (VHH) and High Hazard (HH) classes cover 86.0 % of old
 668 landslides and 91.1% of new landslides, respectively.

669 6 Conclusions

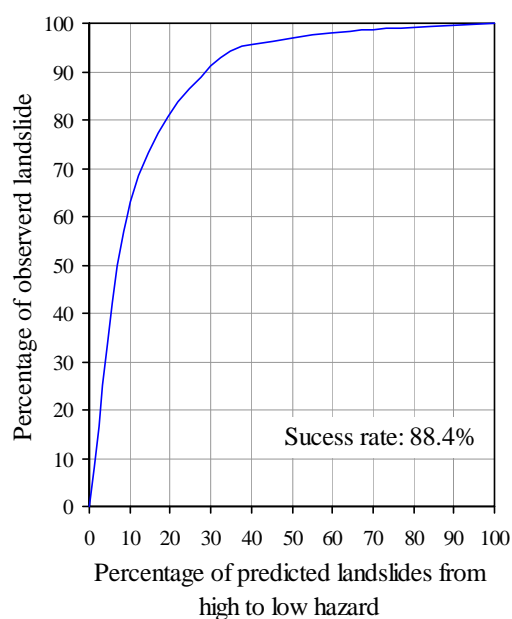
670 Landslide hazard mapping is essential in delineating landslide prone areas in
 671 mountainous regions. Various methodologies have been proposed for landslide
 672 susceptibility and hazard mapping; in this study, weights-of-evidence modelling with
 673 bivariate statistical methods was used because of ease in data acquisition for
 674 modelling. The modelling was applied to the south-western hills of Kathmandu, in the
 675 Lesser Himalaya of Nepal, considering 10 intrinsic factors and one extrinsic factor
 676 affecting landslides. The thematic layers of all causative factors and existing
 677 landslides were prepared in GIS (ILWIS 3.3). Mainly DEM-based causative factors
 678 and field data were used to prepare the data layers of the causative factors. The
 679 conclusions of this study can be summarized as follows:



680

681 Fig 7. Landslide prediction scenarios from high landslide hazard value

- 682 • The landslide hazard value estimated from different time based landslide data and
683 eleven factor maps reveals more or less a similar degree of accuracy ranging from
684 80% to 86%.
- 685 • In many approaches to weights-of-evidence modelling of landslide hazard or
686 susceptibility assessment in GIS, the model validation process is always dependent
687 on the trained landslide data and the same landslide data are used for verification.
688 In contrast, in this study the model was also verified independently with time-
689 based new landslide data and results were very promising, with independent
690 prediction rates of 80% accuracy. This validates weights-of-evidence modelling
691 for landslide hazard assessment on the slopes of the Lesser Himalaya of Nepal.
- 692 • The final landslide hazard map prepared after rectification of older and new
693 landslide-related hazard values was found to be the most acceptable hazard map,
694 with a success rate of 88.4%.
- 695 • The vigorous evaluation of predictive factors used in this modelling suggests that
696 the role of geomorphology and human intervention-related factors is very
697 significant for landslide processes in the Lesser Himalaya of Nepal.
- 698 • The probability values estimated in this kind of predictive modelling are not
699 absolute and represent a relative degree of hazard. However, they can provide an
700 appropriate and valid measure of landslide initiation locality on slopes of the
701 Lesser Himalaya. Likewise, the methodology seems to have extensive
702 applicability in the Lesser Himalaya of Nepal, with the limitation that knowledge
703 of past landslide information affects the final probability values calculated by the
704 model.



705

706 Fig. 8, Success rate curves of final landslide hazard map

707

708

709 Table 3, Distribution of old and new landslides in classified hazard map after weights-of-evidence
710 modeling.

Hazard Classes	Old landslides (%)	New landslides (%)
Very High Hazard (VHH)	59.3	63.1
High Hazard (HH)	26.7	28.0
Moderate Hazard (MH)	8.6	5.9
Low Hazard (LH)	4.8	1.8
711 Very Low Hazard (VLH)	0.6	1.3

712 Acknowledgments

713 We thank Mr. Birendra Piya, senior geologist, Department of Mines and Geology, Government of
714 Nepal, Kathmandu, for his technical assistance. We also acknowledge local community forest user
715 groups of the study area for providing permission to enter the forest for investigation. Mr. Anjan Kumar
716 Dahal and Ms. Seiko Tsuruta are sincerely acknowledged for their technical support during the
717 preparation of this paper. The study has been partly funded by the Sasagawa Fund for Scientific
718 Research, The Japan Science Society.

719 References

- 720 Acharya, K.K., 2001, Geology and structure of the Pharping – Raniban area central Nepal, M. Sc.
721 Thesis, Central Department of Geology, Tribhuvan University, Nepal, Unpublished, 58 pp.
- 722 Agterberg, F.P., Bonham-Carter, G.F., Cheng, Q., Wright, D.F. 1993. Weights of evidence modeling
723 and weighted logistic regression for mineral potential mapping. In: Davis, J.C., Herzfeld, U.C. (eds)
724 Computers in geology, 25 years of progress, Oxford University Press, Oxford, pp 13–32.
- 725 Agterberg, F. P., 1992. Combining Indicator Patterns in Weights of Evidence Modeling for Resource
726 Evaluation, *Natural Resources Research* 1(1), 39–50.
- 727 Anbalagan, D. (1992) Landslide hazard evaluation and zonation mapping in mountainous terrain.
728 *Engineering Geology* 32, 269–277.
- 729 ASTM D 2487-83, Standard classification of soils for engineering purposes (Unified Soil Classification
730 System), ASTM International, 100 Bar, harbor Drive, west Conshohocken, PA 19428, USA.
- 731 Atkinson, P.M., Massari, R., 1998. Generalized linear modelling of landslide susceptibility in the
732 Central Apennines, Italy. *Computer Geoscience* 24(4), 373–385.
- 733 Bonham-Carter, G.F., Agterberg, F. P., Wright, D.F., 1988. Integration of geological datasets for gold
734 exploration in Nova Scotia. *Photogram Eng Remo Sens* 54, 1585–1592.
- 735 Bonham-Carter, G. F., Agterberg, F.P., Wright, D.F., 1989. Weights of evidence modelling: a new
736 approach to mapping mineral potential. *Stat Appl Earth Sci Geol Survey Can Paper* 89–9, 171–183.
- 737 Bonham-Carter, G.F., 2002. Geographic information systems for geoscientist: Modelling with GIS. In:
738 Merriam, D.F. (Ed.), *Computer Methods in the Geosciences*, vol. 13. Pergamon/Elsevier, New York,
739 pp. 302–334.
- 740 Carranza, E. J. M., Hale, M., 2002. Spatial association of mineral occurrences and curvilinear
741 geological features. *Math Geol* 34,203–221.
- 742 Çevik, E., Topal, T., 2003. GIS-based landslide susceptibility mapping for a problematic segment of the
743 natural gas pipeline, Hendek (Turkey), *Environmental Geology* 44, 949–962.

- 744 Cheng, Q., 2004. Application of weights of evidence method for assessment of flowing wells in the
745 Greater Toronto area, Canada. *Natural Resource Research* 13, 77–86.
- 746 Chung, C.-J.F., Fabbri, A.G., 1999. Probabilistic prediction models for landslide hazard mapping,
747 *Photogrammetric Engineering & Remote Sensing* 65(12), 1389–1399.
- 748 Chung, C.-J.F., Fabbri, A. G, 2003. Validation of spatial prediction models for landslide hazard
749 mapping. *Natural Hazards* 30, 451–472.
- 750 Dahal, R.K., 2006a. *Geology for Technical Students - A textbook for Bachelor Level Students*, Bhrikuti
751 Academic Publication, Exhibition Road, Kathmandu, Nepal, 756 pp.
- 752 Dahal, R. K., Hasegawa, S., Yamanaka, M. Nishino, K. 2006b. Rainfall triggered flow-like landslides:
753 understanding from southern hills of Kathmandu, Nepal and northern Shikoku, Japan. *Proc 10th Int*
754 *Congr of IAEG, The Geological Society of London, IAEG2006 Paper number 819 :1-14 (CD-ROM).*
- 755 Dahal, R.K., Hasegawa, S., Nonomura A., Yamanaka, M., Masuda, T., Nishino K., 2007. GIS-based
756 weights-of-evidence modelling of rainfall-induced landslides in small catchments for landslide
757 susceptibility mapping, *Environmental Geology*, Online First. DOI: 10.1007/s00254-007-0818-3, 14
758 pp.
- 759 Dai, F.C., Lee, C.F., Li, J., Xu, Z.W., 2001. Assessment of landslide susceptibility on the natural terrain
760 of Lantau Island, Hong Kong. *Environmental Geology* 40, 381–391.
- 761 Daneshfar, B., Benn, K., 2002. Spatial relationships between natural seismicity and faults, southeastern
762 Ontario and north-central New York state. *Tectonophysics* 353, 31–44.
- 763 Emmanuel, J., Carranza, M., Hale, M., 2000. Geologically constrained probabilistic mapping of gold
764 potential, Baguio district, Philippines. *Natural Resource Research* 9, 237–253.
- 765 Ganser, A., 1964. *Geology of the Himalaya*, Inter Science John Wiley, London, 289 pp.
- 766 Gökceoglu, C., Aksoy, H., 1996. Landslide susceptibility mapping of the slopes in the residual soils of
767 the Mengen region (Turkey) by deterministic stability analyses and image processing techniques,
768 *Engineering Geology* 44, 147–161.
- 769 Greenway, D.R., 1987. Vegetation and slope stability. In: Anderson, M.G., Richards, K.S. (eds.) *Slope*
770 *stability*. Wiley, New York, pp 187–230.
- 771 Guzetti, F., Carrara, A., Cardinali, M., Reichenbach, P., 1999. Landslide hazard evaluation: a review of
772 current techniques and their application in a multi-scale study, central Italy. *Geomorphology* 31, 181–
773 216.
- 774 Harris, J.R., Wilkinson, L., Grunsky, E.C., 2000. Effective use and interpretation of lithogeochemical
775 data in regional mineral exploration programs: application of geographic information systems (GIS)
776 technology. *Ore Geol Rev* 16, 107–143.
- 777 Lee, S., 2004. Application of likelihood Ratio and Logistic Regression Models to Landslide
778 Susceptibility mapping in GIS, *Environmental Management* 34(2), 223–232.
- 779 Lee, S., Choi, J., 2004. Landslide susceptibility mapping using GIS and the weights-of-evidence model.
780 *Int J Geo gr Inf Sci* 18, 789–814.
- 781 Lee, S, Choi, J., Min, K., 2002. Landslide susceptibility analysis and verification using the Bayesian
782 probability model. *Environmental Geology* 43, 120–131
- 783 Lee, S., Min, K., 2001. Statistical analysis of landslide susceptibility at Yongin, Korea. *Environmental*
784 *Geology* 40, 1095–1113.
- 785 Lee, S., Sambath, T., 2006. Landslide susceptibility mapping in the Damrei Romel area, Cambodia
786 using frequency ratio and logistic regression models, *Environmental Geology* 50, 847-855

787 Lee, S., Ryu, J., Kim, I., 2007. Landslide susceptibility analysis and its verification using likelihood
788 ratio, logistic regression and artificial neural network models: case study of Youngin, Korea.
789 Landslides 4(4), 327–338.

790 NAVFAC, 1986. Design manual: soil mechanics, U.S. Dept of Defense, NAVFAC DM-7.01,
791 Department of the Navy, Washington DC, revised version, 389 pp.

792 Neuhäuser, B. Terhorst, G., 2007. Landslide susceptibility assessment using “weights-of-evidence”
793 applied to a study area at the Jurassic escarpment (SW-Germany), *Geomorphology* 86, 12–24.

794 Oguchi, T., 1997. Drainage Density and Relative Relief in Humid Steep Mountains with Frequent
795 Slope Failure , *Earth Surface Processes and Landforms* 22(2), 107–120.

796 Pachauri, A.K., Gupta, P.V., Chander, R., 1998. Landslide zoning in a part of the Garhwal Himalayas.
797 *Environmental Geology* 36, 325–334.

798 Paudel, P.P., Omura, H., Kubota, T., Morita, K., 2003. Landslide damage and disaster management
799 system in Nepal. *Disaster Prevention and Management* 12 (5), 413–419.

800 Paudyal, P., Dhital, M.R., 2005. Landslide hazard and risk zonation of Thankot – Chalnakhel area,
801 central Nepal, *Journal of Nepal Geological Society* 31, 43–50.

802 Remondo, J., González, A., Ramón, J., Cendrero, A., Fabbri, A., Chung, C.-J.F., 2003. Validation of
803 landslide susceptibility maps: examples and applications from a case study in Northern Spain. *Natural*
804 *Hazards* 30, 437–449.

805 Saha, A.K., Gupta, R.P., Sarkar, I., Arora, M.K., Csaplovics, E., 2005. An approach for GIS-based
806 statistical landslide susceptibility zonation - with a case study in the Himalayas, *Landslides* (2), 61–
807 69.

808 Siddle H.J., Jones D.B., Payne H.R., 1991. Development of a methodology for landslip potential
809 mapping in the Rhondda Valley In: Chandler, R.J. (ed.) *Slope Stability Engineering*. London: Thomas
810 Telford. pp. 137-142.

811 Sharma, M., Kumar, R., 2007. GIS-based landslide hazard zonation: a case study from the Parwanoo
812 area, Lesser and Outer Himalaya, H.P., India, *Bull Eng Geol Environ*, Online first, DOI:
813 10.1007/s10064-007-0113-2, 9 pp.

814 Stöcklin, J., Bhattarai, K.D., 1977. Geology of Kathmandu Area and Central Mahabharat Range Nepal
815 Himalaya Kathmandu. HMG/UNDP Mineral Exploration Project, Technical Report, New York, 64
816 pp.

817 Stöcklin, J., 1980. Geology of Nepal and its regional frame, *Journal of the Geological Society London*
818 137, 1-34.

819 Styczen, M.E., Morgan, R.P.C., 1995. Engineering properties of vegetation. In Morgan, R.P.C.,
820 Rickson, R.J. (eds.), *Slope Stabilisation and Erosion Control: a bioengineering approach*, E&FN
821 Spon, London, pp 5-58.

822 Süzen, M.L., Doyuran, V., 2004. A comparison of the GIS based landslide susceptibility assessment
823 methods: multivariate versus bivariate, *Environmental Geology* 45, 665–679.

824 Tangestani, M.H., Moore, F., 2001. Porphyry copper potential mapping using the weights-of-evidence
825 model in a GIS, northern Shahr-e-Babak, Iran. *Aust J Earth Sci* 48, 695–701.

826 Terlien, M.T.J., 1996. Modelling spatial and temporal variations in rainfall-triggered landslides, PhD
827 thesis, ITC Publ. Nr. 32, Enschede, The Netherlands, 254 pp.

828 USBR, 2001. Engineering geology field manual, second edition Vol I, U.S. Department of the Interior
829 Bureau of Reclamation, 432 pp.

- 830 Van Westen, C.J., 2000. The modelling of landslide hazards using GIS, *Survey in Geophysics* 21, 241–
831 255
- 832 Van Westen C.J., Rengers N., Soeters R., 2003. Use of geomorphological information in indirect
833 landslide susceptibility assessment, *Natural Hazards* (30), 399–419.
- 834 Van Westen, C.J., Terlien, T.J., 1996. An approach towards deterministic landslide hazard analysis in
835 GIS. A case study from Manizales (Colombia), *Earth Surf Proc Landforms* 21, 853–868.
- 836 Varnes, D.J., 1984. *Landslide Hazard Zonation: a review of principles and practice*, Commission on
837 landslides of the IAEG, UNESCO, Natural Hazards No. 3, 61 pp.
- 838 Wu, W., Siddle, R.C., 1995. A distributed slope stability model for steep forested basins, *Water*
839 *Resource Research* 31, 2097–2110.
- 840 Yin, K.L., Yan, T.Z., 1988. Statistical prediction model for slope instability of metamorphosed rocks.
841 In: *Proceedings of 5th Int Symp on Landslides, Lausanne, Switzerland* (2), pp 1269–1272.
- 842 Zahiri, H., Palamara, D.R., Flentje, P., Brassington, G.M., Baafi, E., 2006. A GIS-based Weights-of-
843 Evidence model for mapping cliff instabilities associated with mine subsidence, *Environmental*
844 *Geology* 51, 377–386.
- 845 Zêzere, J.L., Rodrigues, M.L., Reis, E., Garcia, R., Oliveira, S., Vieira, G., Ferreira, A.B., 2004. Spatial
846 and temporal data management for the probabilistic landslide hazard assessment considering landslide
847 typology, In *Landslides: Evaluation and Stabilization*, Lacerda, W.A., Ehrlich, M., Fontura, S.A.B.,
848 Sayão, A.S.F (eds), Taylor & Fancis Group, London, V 1, pp 117-123.